ISSN 1392–1320 MATERIALS SCIENCE (MEDŽIAGOTYRA). Vol. XX, No. X. 2025

# The Influence of Scanning Speed on the Multiple Mechanical Properties of Selective Laser Melting Stainless Steel

**Yanmei LI, Chiate LIU *, XingYu ZHAO, Zhibiao YANG, Yebin YANG, Xiaotong CHEN, Qinghua CHEN, Weilin WANG**

*School of Electronic and Electrical Engineering, Zhaoqing University, Ying Bin Avenue, Zhaoqing 526061, Guangdong, China*

http://doi.org/10.5755/j02.ms.38947

*Received 27 September 2024; accepted 2 January 2025*

This study systematically evaluates the tensile strength, impact strength, and microhardness of 316L stainless steel fabricated using selective laser melting (SLM) at varying scanning speeds. The results are also compared with those of traditionally forged 316L stainless steel. The experimental findings indicate that SLM samples exhibit superior ultimate tensile strength, yield strength, and microhardness due to the finer microstructure produced by the rapid cooling rates inherent in SLM processes. However, the increased porosity in SLM samples leads to a reduced elongation to failure and impact toughness compared to traditionally forged 316L stainless steel. Among the SLM samples, those fabricated at higher scanning speeds show higher porosity, resulting in lower impact toughness and a tendency toward brittle fracture. Despite this, there are no significant difference in ultimate tensile strength, yield strength, elongation, or microhardness between samples produced at different scanning speeds. This study enhances our understanding of the microstructure and multiple mechanical properties of SLM materials, laying a practical foundation for further research on their applications.
*Keywords:* selective laser melting, porosity, scanning speed, multiple mechanical properties.

## 1.INTRODUCTION

Selective laser melting (SLM) is an advanced additive manufacturing (AM) technology rooted in powder bed fusion. This process employs a high-energy density laser beam to melt and solidify metal powder layer by layer, transforming a three-dimensional digital model into a solid part. SLM offers greater flexibility in the fabrication complex components compared to traditional manufacturing methods such as forging and casting [1 – 3]. The rapid thermal cycles inherent in the SLM process often result in a finely textured microstructure and non-equilibrium crystal phases [4, 5], but can also induce internal defects within the components. These microstructural characteristics are likely to produce variations in the physical and mechanical properties of components manufactured by SLM compared to those produced by conventional methods.

SLM components' mechanical properties are greatly characterized by the setting of the process parameters. These processing parameters, such as laser power ($P$), scanning speed ($v$), hatch spacing ($h$) and layer thickness ($t$), can converge into a variable of energy, commonly known as volume energy density ($E_v$) as given by Eq. 1 [6]:

$$E_v = \frac{P}{v \times h \times t}. \quad (1)$$

From an energy perspective, when the focused laser beam hits the metal powder at a higher scanning speed, it means that the volume energy density imparted to the powder decreases (assuming other parameters are constant), which will lead to insufficient melting in the molten pool, resulting in defects like porosity and lack of melting after solidification [7, 8]. Additionally, when high scanning speed is combined with low volume energy density, an unstable melting phenomenon occurs in the melt pool, leading to the formation of the well-known balling effect, which is detrimental to the SLM process [9]. Based on these findings, it is clear that scanning speed plays a crucial role in determining the performance of SLM components, which is why it was chosen as the primary parameter in this study.

There are numerous studies in the literature focusing on improving the mechanical properties of SLM 316SS samples by optimizing process parameters and scanning strategy. Liu et al. [10] and Larimian et al. [11] studied the tensile behavior and microhardness of SLM 316L stainless steel under different scanning speeds, laser energy density and scanning strategy. They found that the scanning speed significantly affects densification, microstructure, and mechanical properties. Zhang et al. [12] studied the effects of different parameters on the tensile strength and microhardness of SLM 316L stainless steel, concluding that the optimal placement orientation is perpendicular to the tensile direction, with an optimal hatch scanning angle of approximately 30º. Itziar et al. [13] studied the tensile properties and Charpy impact strength of SLM 316L stainless steel at different manufactured angles, finding that the manufactured angle 30º with regard to XY plane exhibited higher Charpy impact absorbed energy and maximum tensile strength. Salman et al. [14] indicated that the scanning strategy significantly influences the density and grain size, which in turn directly affects the tensile strength of SLM 316L stainless steel samples. Most of

* Corresponding author: C.T. Liu
E-mail: *ctliu1205@gmail.com*

mentioned studies mainly involved tensile strength and microhardness, while research combining these two mechanical properties with impact performance is relatively limited. The aim of this paper is to fill this gap and comprehensively present the multiple mechanical properties of SLM 316L stainless steel.

## 2. MATERIALS AND EXPERIMENT PROCEDURES

### 2.1. Material and methods

The feedstock material used for SLM processing is 316L stainless steel powder manufactured by Xi'an Bo Li Te. Its chemical composition is detailed in Table 1. The scanning electron microscopy (SEM) morphology of the spherical powder is shown in Fig. 1 a, with a particle size distribution, ranging from 12.4 μm to 55.4 μm, as depicted in Fig. 1 b.

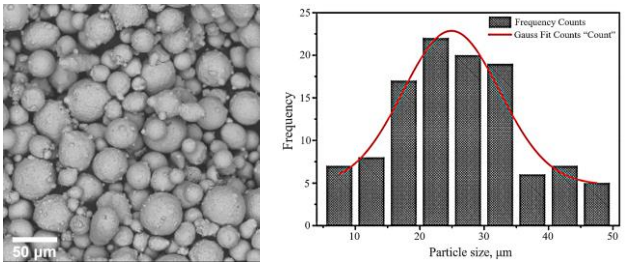


a b

**Fig. 1.** a – SEM morphology; b – particle size distribution of the feedstock powder [15]

**Table 1.** The chemical composition of 316L stainless steel powder, wt.%

| S | P | C | Si | Mn | Mo | Ni | Cr | Fe |
|---|---|---|---|---|---|---|---|---|
| 0.005 | 0.02 | 0.02 | 0.71 | 1.19 | 2.2 | 10.3 | 16.8 | Bal. |

SLM-316L stainless steel samples (hereafter referred to as SLM-316L) were fabricated using the BLT-S200 SLM forming equipment, which is equipped with a 200W laser and features a powder bed layer. The laser equipment BLT-S200 is a continuous wave laser with a wavelength of 1060 – 1080 nm. A zoning strip scanning strategy was employed, and the samples were built along the vertical direction. Two sets of samples were prepared: one at a low scanning speed of 800 mm/s and the other at a high scanning speed of 1600 mm/s (hereafter referred to as LSLM-316L and HSLM-316L samples, respectively). The specific parameters are listed in Table 2. For comparison, traditionally forged 316L stainless steel (TF-316L) after heat treatment at 1100 °C for 2 hours followed by air cooling, was used as the reference material.

**Table 2.** The SLM samples processing parameters

| Samples | Laser power, W | Hatch spacing, μm | Layer thickness, μm | Scanning speed, mm/s |
|---|---|---|---|---|
| LSLM-316L | 135 | 80 | 20 | 800 |
| HSLM-316L | 135 | 80 | 20 | 1600 |

### 2.2. Characterization

Phase characterization of SLM samples is measured using a Bruker D8 Advance X-ray diffractometry (XRD). The device uses Cu-Kα radiation from 40° to 95° with scan speed of 10°/min scanning speed. The microstructures were observed by using a Phenom ProX scanning electron microscopy (SEM). The metallographic preparation of the samples involved cutting, followed by hot mounting, grinding, and polishing. A reagent consisting of $HNO_3$ and HCl in the ratio of 1:3 was used as etching solution.

### 2.3. Tensile tests

The specimen for the tensile tests was machined from the SLM fabricated plates. The tensile properties were determined using the Shanghai Qingji QJ212 metal tensile testing machine (with a capacity of 50 kN and an accuracy of 0.5 grade) at room temperature. The test method followed the ASTM E8/E8M-09 standard [16]. During the experiment, the ultimate tensile strength (UTS), yield strength (YS), and elongation to failure (El) were measured and recorded simultaneously.

### 2.4. Charpy impact tests

The Charpy impact test was carried out using a Tinius Olsen NI300 impact testing machine (with a capacity of 1kN and an impact energy of 300 J). The testing method followed the ASTM E23 standard [17]. Three batches of standardized specimens were also manufactured by SLM. Each specimen had dimension of 55 mm × 10 mm × 10 mm, and a V-shaped notch with a depth of 2 mm. The test data were collected from three specimens, and the final impact energy value was determined by averaging the results of these tests.

### 2.5. Microhardness tests

The microhardness was measured by HVD-1000IS Vickers hardness tester produced by Shanghai Jujing, with a load of 0.2 kg and dwell time of 15 sesonds. Each microhardness value represents the average of three measurement.

## 3. RESULTS AND DISCUSSION

### 3.1. Microstructure characterizations

Fig. 2 presents the XRD diffraction patterns of 316L stainless steel (SS) powder and SLM-316L samples produced at different scanning speeds. The XRD results for the 316L SS powder align with previous studies [18], indicating a fully γ-phase structure. On the contrary, the diffraction peaks of the SLM samples reveal the presence of not only the γ phase but also some $\delta$ phases at lower angle positions. This phenomenon occurs because the high cooling rate during the SLM process inhibits the complete transformation of $\delta$ phases into $\gamma$ phases [19]. Additional differences in the $\delta$ phase peaks between LSLM-316L and HSLM-316L samples have been discussed in previous research [15].

Fig. 3 displays SEM images of the SLM-316L samples fabricated at two different scanning speeds. As shown in Fig. 3 a and b, LSLM-316L samples exhibit distinct directional melt traces compared to the HSLM-316L samples. Furthermore, the HSLM-316L samples show a notable distribution of pores with varying sizes and irregular

shapes, some of which contain unmelted powder, whereas the LSLM-316L samples predominantly feature spherical pores.

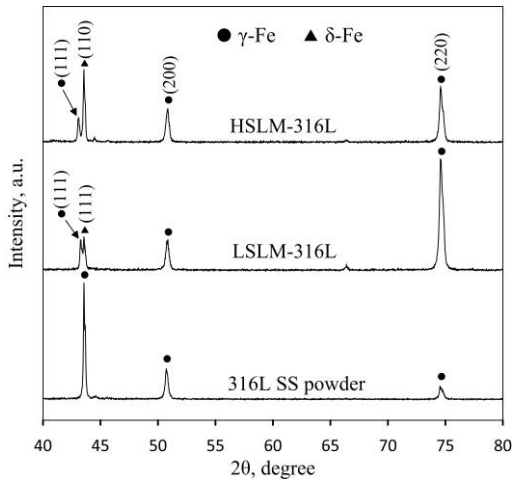


**Fig. 2.** XRD patterns of 316L SS powder and SLM-316L samples

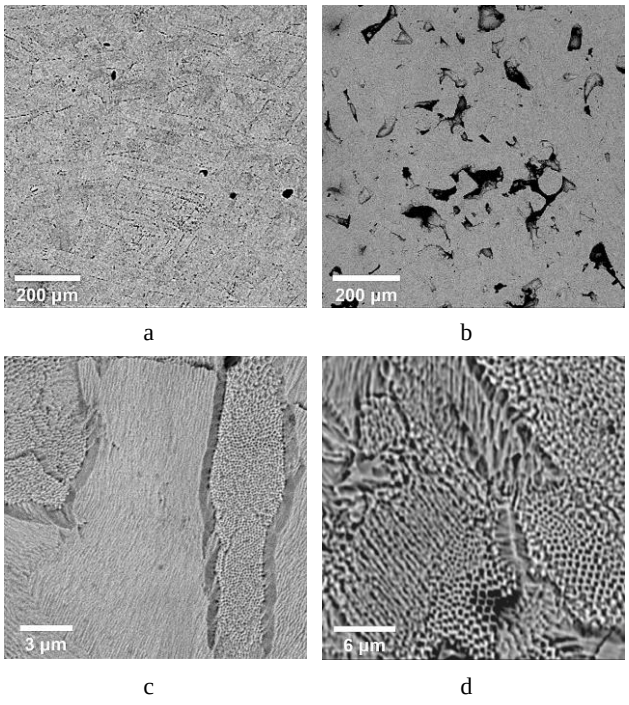


**Fig. 3.** The microstructures: a, c – LSLM-316L sample; b, d – HSLM-316L sample

These observations suggest that the higher scanning speed results in insufficient dwell time of the melt pool, leading to inadequate laser energy, incomplete melting of powder particles, and a lack of fusion between adjacent tracks [20].

In-depth examination reveals a cellular microstructure composed of fine anisotropic equiaxed grains and isotropic columnar grains in both samples, as shown in Fig. 3 c and d. These microstructural features are mainly influenced by the thermal gradient (G) and rapid solidification rate (R) during the SLM process. In theory, the G/R ratio plays a crucial role in determining the morphology of the solidified structure. As the G/R ratio increases, the crystal morphology transitions from equiaxed to dendritic, cellular, and planar crystals [21, 22]. Therefore, it can be clearly seen that due to the faster cooling rate and less higher thermal gradient, the HSLM-316L samples exhibit denser and higher proportion of fine equiaxed grains compared to the LSLM-316L samples.

### 3.2. Defect types and porosity calculation

There are notable differences in defect morphology between the LSLM-316L and HSLM-316L samples. The defects in LSLM-316L samples primarily consist of spherical pores, as illustrated in Fig. 3 a. These defects are typically caused by the keyhole effect or the entrapment of gas bubbles [23]. On the contrary, HSLM-316L samples exhibit irregularly shaped pores of varying sizes, with some exceeding 100 μm, as shown in Fig. 3 b. These defects, including lack of fusion, spatter rejection, and voids, are mainly attributed to process-related issues and are commonly referred to as process-induced porosity [24].

To quantify the porosity of the samples, this study employed the formula described in previous research [25, 26] to calculate the porosity. The formula is as follows:

$$p_r(\%) = \left[1 - \left(\frac{\sigma_a}{\sigma_s}\right)\right] \times 100, \quad (2)$$

where $\sigma_s$ is the theoretical density of 316L SS (7.985 g/cm³), $\sigma_a$ is the measured density of the tested samples obtained using the Archimedes method. Fig. 4 shows the mean porosity and density values, derived from three measurements for each sample. The results indicate that the porosity of the TF-316L samples is significantly lower than that of the SLM-316L samples, with a value of 0.67 %. Among the SLM samples, HSLM-316L exhibits the highest porosity at 2.96 %, while LSLM-316L has a porosity less than half that of HSLM-316L, at 1.33 %. These findings are consistent with the microscopic observations from the SEM images presented in Fig. 3.

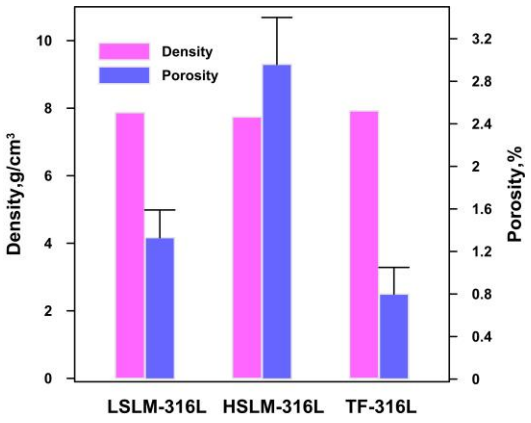


**Fig. 4.** The porosity and density of SLM-316L and TF-316L samples

### 3.3. Tensile strength

Fig. 5 displays the stress-strain curves for the SLM-316L and TF-316L samples subjected to the axial tension test. The ultimate tensile strength (UTS), the yield strength (YS), and the elongation to failure (El) of these samples are summarized in Table 3. The results indicate that the SLM-316L samples exhibit significantly higher UTS and YS compared to the TF-316L samples. This improvement is attributed to the faster cooling rates associated with higher

scanning speeds during the SLM process, which result in finer microstructures and enhanced mechanical properties.

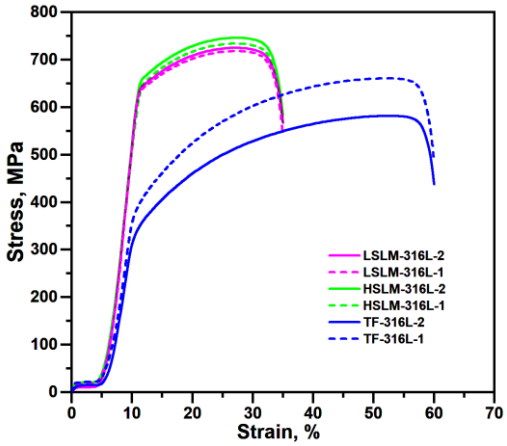


**Fig. 5.** Tensile stress-strain curves of the SLM-316L and TF-316L samples

The increased density of grain boundaries in samples with finer microstructures impedes dislocation slip, thereby improving both yield and ultimate tensile strength.

Furthemore , the UTS and YS of HSLM-316L samples are slightly higher than those of LSLM-316L samples. This enhancement is likely due to the higher proportion of equiaxed grains in HSLM-316L samples, as previous studies have shown that a greater proportion of equiaxed grains contributes to higher tensile strength [27, 28]. Despite the superior UTS and YS of SLM-316L samples relative to TF-316L, their elongation to failure (El) values are relatively low. This is primarily due to the higher porosity in SLM-316L samples, which reduces their plasticity and affects its elongation performance. Specifically, the elongation values for LSLM-316L and HSLM-316L are similar, approximately 34 % and 35 %, respectively. This similarity indicates that porosity plays a critical role in governing the ductility of SLM-316L samples.

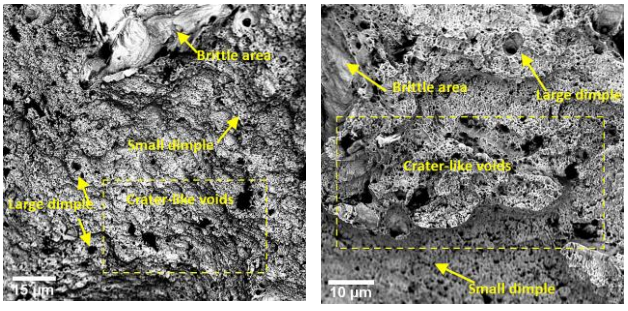


a b

**Fig. 6.** Fracture morphologies: a – LSLM-316L; b – HSLM-316L samples after tensile tests

The fracture morphologies of LSLM-316L and HSLM-316L samples after tensile tests are shown in Fig. 7. It can be observed that some crater-like voids are randomly distributed on the fracture surfaces on both samples (highlighted within the yellow dashed lines). These voids result from partially melted or unmelted powder granules trapped between the melt pools during the SLM process. During tensile testing, these granules contribute to the formation of crater-like voids with irregular shapes and sharp angles, which exacerbate local stress concentration and crack propagation [29]. This phenomenon helps explain the observed reduction in elongation to failure for both samples.

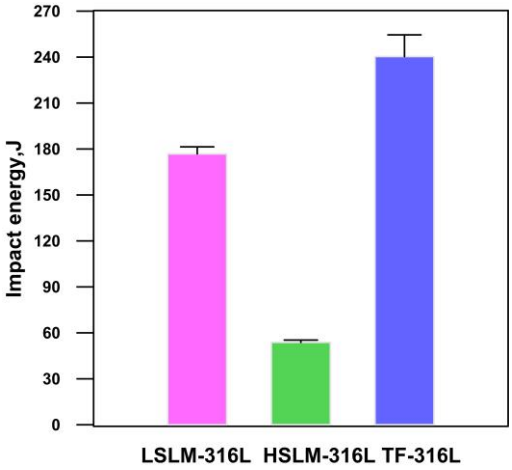


**Fig. 7.** Impact energy and corresponding porosity of the SLM-316L and TF-316L samples

Additionally, the fracture surface also shows characteristics of both ductile-fracture (highlighted large and small dimples) and brittle-fracture (highlighted brittle area with insufficient plastic deformation) on both samples. Thus, the fracture behavior of the LSLM-316L and HSLM-316L samples can be characterized as a combination of ductile and brittle mechanisms.

**Table 3.** Mechanical properties of the SLM-316L and TF-316L samples after tensile tests

| | LSLM-316L | HSLM-316L | TF-316L |
|---|---|---|---|
| YS, MPa | 676±0.5 | 682±0.4 | 420±0.5 |
| UTS, MPa | 732±0.1 | 713±0.9 | 602±0.5 |
| El, % | 35 | 34 | 60 |

## 3.4. Impact strength

The Charpy V-notch impact test is commonly used to evaluate the toughness of metallic materials. In this study, this test was employed to assess the impact toughness of the SLM-316L samples at room temperature and compare them with the TF-316L samples.

From the results shown in Fig. 7, it can be observed that the average impact absorption energy of the LSLM-316L samples is 176.8 J, which is much higher than that of the HSLM-316L samples (53.8 J). However, both SLM-316L samples exhibit significantly lower impact toughness compared to TF-316L samples (240.4 J). A comparison of impact energy and porosity reveals that lower porosity correlates with higher impact absorption energy, highlighting the dominant role of porosity in influencing impact performance.

Fig. 8 illustrates the fracture surface morphologies of impact tested samples. It can be observed clearly that the TF-316L samples, with lowest porosity, exhibit completely typical ductile fracture characteristics compared to the SLM-316L samples. As for the SLM-316L samples, the LSLM-316L samples exhibit plastic deformation to some extent and with partial ductile fracture characteristics. In

contrast, the HSLM-316L samples show a flat fracture face indicative of a brittle fracture. These observations are consistent with the impact test results presented in Fig. 7.

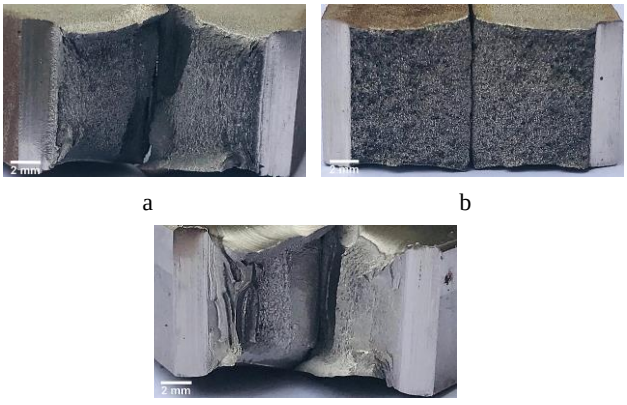


**Fig. 8.** Fracture morphologies: a – LSLM-316L; b – HSLM-316L; c – TF-316L samples after impact tests

### 3.5. Microhardness

Vickers microhardness measurements of SLM-316L samples are shown in Fig. 9, with TF-316L samples included for reference. The results indicate that the average microhardness values for SLM-316L samples are notably higher than those for TF-316L samples, with LSLM-316L samples showing 286.8 HV and HSLM-316L samples showing 270 HV, compared to 207.2 HV for TF-316L samples.

When comparing microhardness with porosity, it is apparent that microhardness values are not significantly affected by porosity but are closely related to the grain size of the microstructure formed by different manufacturing methods. This observation aligns with the Hall-Petch relationship, which suggests that smaller grain sizes lead to increased hardness [10].

The differences in microhardness between the LSLM-316L and HSLM-316L samples are relatively minor. The large deviation of both microhardness values, as depicted in the figure, may be attributed to factors such as the random selection of testing areas, uneven distribution of defects, and the number of samples tested. Further research and verification are ongoing to confirm these findings.

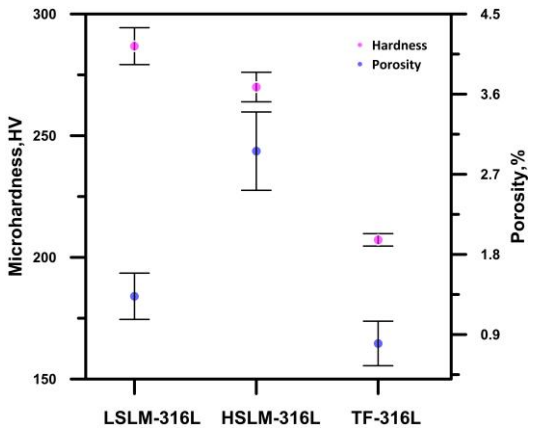


**Fig. 9.** Vickers microhardness of SLM-316L and TF-316L samples

## 4. CONCLUSIONS

In this study, the influence of scanning speed on the mechanical properties of 316L stainless steel (SS) fabricated by SLM was evaluated and compared with traditionally forged 316L SS. The study highlights two primary effects induced by varying scanning speeds: changes in microstructure and generation of porosity. The major conclusions can be summarized as follows:

1. The ultimate tensile strength (UTS) and yield strength (YS) of the SLM-316L samples are significantly higher than those of traditionally forged TF-316L samples. This enhancement is attributed to the finer microstructures resulting from rapid cooling rates during SLM. Among the SLM samples, HSLM-316L exhibits slightly higher UTS and YS compared to LSLM-316L, likely due to a higher proportion of equiaxed grains in HSLM-316L.
2. The elongation to failure (El) of the SLM-316L samples is lower compared to the TF-316L samples, primarily due to increased porosity in the SLM samples. Defects such as lack of fusion, voids, and pores observed in microstructures significantly influence the fracture behavior of the SLM-316L samples.
3. The impact absorption energy of SLM-316L samples is significantly lower than that of TF-316L samples, due to the higher porosity in the SLM samples. A similar porosity effect also led to LSLM-316L samples with higher impact energy compared to HSLM-316L samples, indicating that porosity plays a crucial role in affecting impact toughness.
4. Vickers microhardness values for SLM-316L samples are considerably higher than those for TF-316L samples. The difference in microhardness between the LSLM-316L and HSLM-316L samples is minimal, suggesting that microstructure refinement has a more significant impact on microhardness than porosity.


### *Acknowledgments*

The authors thank the financial support from Zhaoqing University's Horizontal Research Project (KJ20230605H054).


#### REFERENCES


1. **Zhang, H., Zhu, H., Qi, T., Hu, Z., Zeng, X.** Selective Laser Melting of High Strength Al–Cu–Mg Alloys: Processing, Microstructure and Mechanical Properties *Materials Science and Engineering: A* 656 2016: pp. 47 – 54. https://doi.org/10.1016/j.msea.2015.12.101
2. **Krakhmalev, P., Yadroitsava, I., Fredriksson, G., Yadroitsev, I.** In Situ Heat Treatment in Selective Laser Melted Martensitic AISI 420 Stainless Steels *Materials & Design* 87 2015: pp. 380 – 385. https://doi.org/10.1016/j.matdes.2015.08.045
3. **Parry, L., Ashcroft, I.A., Wildman, R.D.** Understanding the Effect of Laser Scan Strategy on Residual Stress in Selective Laser Melting through Thermo-Mechanical Simulation *Additive Manufacturing* 12 2016: pp. 1 – 15. https://doi.org/10.1016/j.addma.2016.05.014
4. **Prashanth, K.G., Scudino, S., Klauss, H.J., Surreddi, K.B., Löber, L., Wang, Z., Chaubey, A.K., Kühn, U., Eckert, J.** Microstructure and Mechanical Properties of Al–12Si

Produced by Selective Laser Melting: Effect of Heat Treatment *Materials Science and Engineering: A* 590 2014: pp. 153 – 160. https://doi.org/10.1016/j.msea.2013.10.023

5. **Hanzl, P., Zetek, M., Bakša, T., Kroupa, T.** The Influence of Processing Parameters on the Mechanical Properties of SLM Parts *Procedia Engineering* 100 2015: pp. 1405 – 1413. https://doi.org/10.1016/j.proeng.2015.01.510
6. **Choi, J.P., Shin, G.H., Brochu, M., Kim, Y.J., Yang, S.S., Kim, K.T., Yang, D.Y., Lee, C.W., Yu, J.H.** Densification Behavior of 316L Stainless Steel Parts Fabricated by Selective Laser Melting by Variation in Laser Energy Density *Materials Transactions* 57 (11) 2016: pp. 1952 – 1959. https://doi.org/10.2320/matertrans.M2016284
7. **Carlton, H.D., Haboub, A., Gallegos, G.F., Parkinson, D.Y., MacDowell, A.A.** Damage Evolution and Failure Mechanisms in Additively Manufactured Stainless Steel *Materials Science and Engineering: A* 651 2016: pp. 406 – 414. https://doi.org/10.1016/j.msea.2015.10.073
8. **Liu, Q., Elambasseril, J., Sun, S., Leary, M., Brandt, M., Sharp, P.** The Effect of Manufacturing Defects on the Fatigue Behaviour of Ti-6Al-4V Specimens Fabricated Using Selective Laser Melting *Advanced Materials Research* 891 – 892 2014: pp. 1519 – 1524. https://doi.org/10.4028/www.scientific.net/AMR.891-892.1519
9. **Gunenthiram, V., Peyre, P., Schneider, M., Dal, M., Coste, F., Koutiri, I., Fabbro, R.** Experimental Analysis of Spatter Generation and Melt-Pool Behavior During the Powder Bed Laser Beam Melting Process *Journal of Materials Processing Technology* 251 2018: pp. 376 – 386. https://doi.org/10.1016/j.jmatprotec.2017.08.012
10. **Liu, J., Song, Y., Chen, C., Wang, X., Li, H., Zhou, C.A., Wang, J., Guo, K., Sun, J.** Effect of Scanning Speed on the Microstructure and Mechanical Behavior of 316L Stainless Steel Fabricated by Selective Laser Melting *Materials & Design* 186 2020: pp. 108355. https://doi.org/10.1016/j.matdes.2019.108355
11. **Larimian, T., Kannan, M., Grzesiak, D., AlMangour, B., Borkar, T.** Effect of Energy Density and Scanning Strategy on Densification, Microstructure and Mechanical Properties of 316L Stainless Steel Processed Via Selective Laser Melting *Materials Science and Engineering: A* 770 2020: pp. 138455. https://doi.org/10.1016/j.msea.2019.138455
12. **Zhang, Z., Chu, B., Wang, L., Lu, Z.** Comprehensive Effects of Placement Orientation and Scanning Angle on Mechanical Properties and Behavior of 316L Stainless Steel Based on the Selective Laser Melting Process *Journal of Alloys and Compounds* 791 2019: pp. 166 – 175. https://doi.org/10.1016/j.jallcom.2019.03.082
13. **Tolosa, I., Garciandía, F., Zubiri, F., Zapirain, F., Esnaola, A.** Study of Mechanical Properties of AISI 316 Stainless Steel Processed by "Selective Laser Melting", Following Different Manufacturing Strategies *The International Journal of Advanced Manufacturing Technology* 51 (5) 2010: pp. 639 – 647. https://doi.org/10.1007/s00170-010-2631-5
14. **Salman, O.O., Brenne, F., Niendorf, T., Eckert, J., Prashanth, K.G., He, T., Scudino, S.** Impact of the Scanning Strategy on the Mechanical Behavior of 316L Steel Synthesized by Selective Laser Melting *Journal of Manufacturing Processes* 45 2019: pp. 255 – 261. https://doi.org/10.1016/j.jmapro.2019.07.010
15. **Li, Y., Liu, C., Liang, Y., Chen, X., Yang, Z., Chen, Y.** The Long-Term Corrosion Behaviors of SLM 316L Stainless Steel Immersed in Artificial Saliva *Materials Science (Medžiagotyra)* 28 (2) 2021: pp. 196 – 201. https://doi.org/10.5755/j02.ms.28636
16. **ASTM International.** ASTM E8/E8M-Standard Test Methods for Tension Testing of Metallic Materials *Annu B ASTM Stand* 2010: pp. 1 – 27. https://doi.org/10.1520/E0008_E0008M-22
17. **ASTM International.** ASTM E23: Standard Test Methods for Notched Bar, Impact Testing of Metallic Materials *Annu B ASTM Stand* 2012: pp. 1 – 26. https://doi.org/10.1520/E0023-18
18. **Zhong, Y., Liu, L., Wikman, S., Cui, D., Shen, Z.** Intragranular Cellular Segregation Network Structure Strengthening 316L Stainless Steel Prepared by Selective Laser Melting *Journal of Nuclear Materials* 470 2016: pp. 170 – 178. https://doi.org/10.1016/j.jnucmat.2015.12.034
19. **Sun, Z., Tan, X., Tor, S.B., Yeong, W.Y.** Selective Laser Melting of Stainless Steel 316L with Low Porosity and High Build Rates *Materials & Design* 104 2016: pp. 197 – 204. https://doi.org/10.1016/j.matdes.2016.05.035
20. **Oliveira, J.P., Santos, T.G., Miranda, R.M.** Revisiting Fundamental Welding Concepts to Improve Additive Manufacturing: From Theory to Practice *Progress in Materials Science* 107 2020: pp. 100590. https://doi.org/10.1016/j.pmatsci.2019.100590
21. **Liu, W., Liu, C.S., Wang, Y., Zhang, H., Li, J., Lu, Y.Y., Xiong, L., Ni, H.W.** Tailoring the Microstructural and Mechanical Properties of 316L Stainless Steel Manufactured by Laser Powder Bed Fusion *Journal of Materials Research and Technology* 25 2023: pp. 7389 – 7405. https://doi.org/10.1016/j.jmrt.2023.07.158
22. **Duan, H., Liu, B., Fu, A., He, J., Yang, T., Liu, C.T., Liu, Y.** Segregation Enabled Outstanding Combination of Mechanical and Corrosion Properties in a FeCrNi Medium Entropy Alloy Manufactured by Selective Laser Melting *Journal of Materials Science & Technology* 99 2022: pp. 207 – 214. https://doi.org/10.1016/j.jmst.2021.05.018
23. **Pal, S., Finšgar, M., Hudák, R., Rajťúková, V., Brajlih, T., Gubeljak, N., Drstvenšek, I.** Mechanisms of Defect Formation in Ti-6Al-4V Product During Re-Melting of Layers in Selective Laser Melting *Journal of Manufacturing Processes* 105 2023: pp. 260 – 275. https://doi.org/10.1016/j.jmapro.2023.09.044
24. **Sames, W.J., List, F.A., Pannala, S., Dehoff, R.R., Babu, S.S.** The Metallurgy and Processing Science of Metal Additive Manufacturing *International Materials Reviews* 61 (5) 2016: pp. 315 – 360. https://doi.org/10.1080/09506608.2015.1116649
25. **Spierings, A.B., Schneider, M., Eggenberger, R.** Comparison of Density Measurement Techniques for Additive Manufactured Metallic Parts *Rapid Prototyping Journal* 17 (5) 2011: pp. 380 – 386. https://doi.org/10.1108/13552541111156504
26. **De Terris, T., Andreau, O., Peyre, P., Adamski, F., Koutiri, I., Gorny, C., Dupuy, C.** Optimization and Comparison of Porosity Rate Measurement Methods of Selective Laser Melted Metallic Parts *Additive Manufacturing* 28 2019: pp. 802 – 813. https://doi.org/10.1016/j.addma.2019.05.035
27. **Li, Y., Ma, C., Qin, F., Chen, H., Zhao, X., Liu, R., Gao, S.** The Microstructure and Mechanical Properties of 316L

Austenitic Stainless Steel Prepared by Forge and Laser Melting Deposition *Materials Science and Engineering: A* 870 2023: pp. 144820. https://doi.org/10.1016/j.msea.2023.144820

28. **Xiong, W., Hao, L., Peijs, T., Yan, C., Cheng, K., Gong, P., Cui, Q., Tang, D., Al Islam, S., Li, Y.** Simultaneous Strength and Ductility Enhancements of High Thermal Conductive Ag7.5Cu Alloy by Selective Laser Melting *Scientific Reports* 12 (1) 2022: pp. 4250. https://doi.org/10.1038/s41598-022-08182-4
29. **Sohrabpoor, H., Salarvand, V., Lupoi, R., Chu, Q., Li, W., Aldwell, B., Stanley, W., O'Halloran, S., Raghavendra, R., Choi, C.H., Brabazon, D.** Microstructural and Mechanical Evaluation of Post-Processed SS 316L Manufactured by Laser-Based Powder Bed Fusion *Journal of Materials Research and Technology* 12 2021: pp. 210 – 220. https://doi.org/10.1016/j.jmrt.2021.02.090